Journal of Advanced Research 52 (2023) 219–232

Contents lists available at ScienceDirect

Journal of Advanced Research

journal homepage: www.elsevier.com/locate/jare

Original Article

Targeting *Desulfovibrio vulgaris* flagellin-induced NAIP/NLRC4 inflammasome activation in macrophages attenuates ulcerative colitis

Yaping An [1], Zihan Zhai [1], Xin Wang [1], Yiyun Ding [1], Linlin He, Lingfeng Li, Qi Mo, Chenlu Mu, Runxiang Xie, Tianyu Liu, Weilong Zhong, Bangmao Wang, Hailong Cao *

Department of Gastroenterology and Hepatology, General Hospital, Tianjin Medical University, National Key Clinical Specialty, Tianjin Institute of Digestive Diseases, Tianjin Key Laboratory of Digestive Diseases, Tianjin, China

HIGHLIGHTS

- *D. vulgaris* was enriched in UC patients.
- *D. vulgaris* or its flagellin facilitated the DSS-induced colitis in mice.
- DVF facilitated inflammation by activating NAIP/NLRC4 inflammasome and inducing macrophage pyroptosis.
- Eugeniin targeted the interaction between DVF and NAIP and attenuated the DVF-induced proinflammatory effect.

GRAPHICAL ABSTRACT

Targeting *Desulfovibrio vulgaris* flagellin-induced NAIP/NLRC4 inflammasome activation and macrophage pyroptosis attenuates ulcerative colitis. Overgrowth of *D. vulgaris* containing flagellin destroyed the intestinal barrier, which disrupted epithelial cells and tight junctions to promote the bacterial translocation into lamina propria. *D. vulgaris* flagellin (DVF) could interact with the NAIP protein, which can be blocked by eugeniin as the interface targeting inhibitor. The persistent activation of NAIP/NLRC4 inflammasome induces macrophage pyroptosis mediated by caspase1-dependent cleavage of GSDMD and releases proinflammatory cytokines including IL-1β and IL-18, facilitating the occurrence and progression of UC. NAIP: NLR family of apoptosis inhibitory proteins; NLRC4: NLR family caspase activation and recruitment domain-containing protein 4; DVF: *Desulfovibrio vulgaris* flagellin; GSDMD: Gasdermin D.

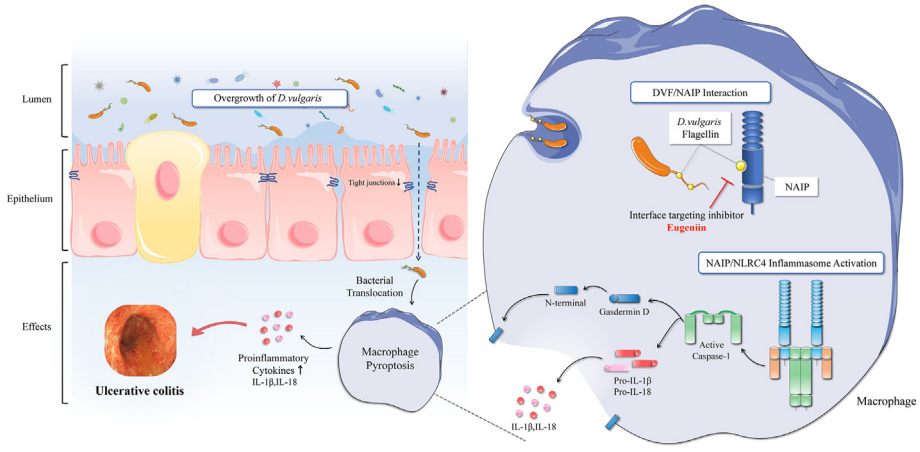

Abbreviations: ASC, apoptosis-associated speck-like protein containing a CARD; DAI, disease activity index; DAMPs, damage-associated molecular patterns; DAPI, 40,6-diamidino-2-phenylindole; DSS, dextran sulfate sodium; DSV, *D. vulgaris*, *Desulfovibrio vulgaris*; DVF, *D. vulgaris* flagellin; GO, Gene Ontology; GSDMD, gasdermin D; HC, healthy controls; HDC, histidine decarboxylase; hNAIP, NAIP protein encoded by human genome; IBD, inflammatory bowel disease; IL, interleukin; KEGG, Kyoto Encyclopedia of Genes and Genomes; LDH, lactate dehydrogenase; MAS, macrophage activation syndrome; NAIPs, NLR family of apoptosis inhibitory proteins; NLRC4, NLR family caspase activation and recruitment domain-containing protein 4; NLRP3, NOD-like receptor pyrin domain containing 3; NLRs, nucleotide-binding oligomerization domain-like receptors; NO, nitric oxide; PAMPs, pathogen-associated molecular patterns; PBS, phosphate-buffered saline; PGE2, prostaglandin E2; PI, propidium iodide; PVDF, polyvinylidene fluoride; qPCR, quantitative PCR; SPF, specific pathogen-free; SRB, sulfate reducing bacteria; T3SS, type III secretion system; UC, ulcerative colitis.

* Corresponding author at: Department of Gastroenterology and Hepatology, General Hospital, Tianjin Medical University, Tianjin 300052, China.
E-mail address: caohailong@tmu.edu.cn (H. Cao).

[1] These authors contributed equally to this work.

https://doi.org/10.1016/j.jare.2023.08.008

ARTICLE INFO

Article history:
Received 15 December 2022
Revised 11 August 2023
Accepted 13 August 2023
Available online 15 August 2023

Keywords:
Ulcerative colitis
Desulfovibrio vulgaris
NAIP/NLRC4 inflammasome
Pyroptosis
Eugeniin

ABSTRACT

Introduction: The perturbations of gut microbiota could interact with excessively activated immune responses and play key roles in the etiopathogenesis of ulcerative colitis (UC). *Desulfovibrio*, the most predominant sulfate reducing bacteria (SRB) resided in the human gut, was observed to overgrow in patients with UC. The interactions between specific gut microbiota and drugs and their impacts on UC treatment have not been demonstrated well.

Objectives: This study aimed to elucidate whether *Desulfovibrio vulgaris* (*D. vulgaris*, DSV) and its flagellin could activate nucleotide-binding oligomerization domain-like receptors (NLR) family of apoptosis inhibitory proteins (NAIP) / NLR family caspase activation and recruitment domain-containing protein 4 (NLRC4) inflammasome and promote colitis, and further evaluate the efficacy of eugeniin targeting the interaction interface of *D. vulgaris* flagellin (DVF) and NAIP to attenuate UC.

Methods: The abundance of DSV and the occurrence of macrophage pyroptosis in human UC tissues were investigated. Colitis in mice was established by dextran sulfate sodium (DSS) and gavaged with DSV or its purified flagellin. NAIP/NLRC4 inflammasome activation and macrophage pyroptosis were evaluated *in vivo* and *in vitro*. The effects of eugeniin on blocking the interaction of DVF and NAIP/NLRC4 and relieving colitis were also assessed.

Results: The abundance of DSV increased in the feces of patients with UC and was found to be associated with disease activity. DSV and its flagellin facilitated DSS-induced colitis in mice. Mechanistically, RNA sequencing showed that gene expression associated with inflammasome complex and pyroptosis was upregulated after DVF treatment in macrophages. DVF was further demonstrated to induce significant macrophage pyroptosis *in vitro*, depending on NAIP/NLRC4 inflammasome activation. Furthermore, eugeniin was screened as an inhibitor of the interface between DVF and NAIP and successfully alleviated the proinflammatory effect of DVF in colitis.

Conclusion: Targeting DVF-induced NAIP/NLRC4 inflammasome activation and macrophage pyroptosis ameliorates UC. This finding is of great significance for exploring the gut microbiota-host interactions in UC development and providing new insights for precise treatment.

Introduction

Ulcerative colitis (UC) is a nonspecific chronic inflammatory disorder characterized by recurrent and diffuse mucosal inflammation of the colorectum [1,2], with progressively increasing incidence and prevalence over time. Current evidence has suggested that UC is attributed to a confluence of genetic susceptibilities and environmental factors and can alter gut homeostasis and trigger immune response mediated inflammation [3], but the pathogenesis of the disease remains unclear. The interactions between gut microbiota and host have been attested to be vital in UC progression [4,5]. *Desulfovibrio* spp. is a predominant sulfate reducing bacteria (SRB) that resides in the human gut [6], the number of SRB often increases under conditions associated with microbial dysbiosis and inflammatory conditions [7,8]. Studies found that SRB aggravated inflammation in experimental colitis by stimulating the gut immune responses [9] and producing hydrogen sulfide and acetate [10]. *Desulfovibrio vulgaris* (*D. vulgaris*, DSV) induced the aberrant localization of tight junction proteins and increased the permeability of intestinal epithelial barrier [11]. However, the underlying mechanisms of DSV in interacting with the host and modulating intestinal inflammation remain unclear.

Inflammasomes are a cluster of intracellular multiprotein platforms that respond to pathogen-associated molecular patterns (PAMPs) or damage-associated molecular patterns (DAMPs), which initiate appropriate and necessary immune reactions and inflammatory cascades to maintain the homeostasis of the gastrointestinal tract [12]. Inflammasomes are triggered by several nucleotide-binding oligomerization domain-like receptors (NLRs), a protein family with diverse functions [13]. The NLR family of apoptosis inhibitory proteins (NAIPs) can recruit adaptor NLR family caspase activation and recruitment domain-containing protein 4 (NLRC4) and form NAIP/NLRC4 inflammasome, which reacts to cytoplasmic flagellin, the needle and inner rod proteins from bacterial type III secretion system (T3SS) [14]. NAIP1 and NAIP2 detect the needle and inner rod proteins, respectively, while NAIP5/6 recognize the cytosolic flagellin in mice. The human genome only encodes a single functional NAIP protein (hNAIP), which mediates responses to T3SS components and flagellin [15]. The activation of inflammasome complex triggers caspase-1-mediated proteolytic cleavage of the pore-forming protein gasdermin D (GSDMD) due to pyroptosis and then releases proinflammatory cytokines, namely, interleukin (IL)-1β and IL-18 [16,17]. The localized effects of NAIP/NLRC4 inflammasome could defend against bacterial pathogens [18], but the aberrant activity of this cluster also leads to multiple clinical manifestations, including macrophage activation syndrome, neonatal enterocolitis, and UC [19–21].

Myeloid cells, predominantly macrophages, are the major targets of inflammasome and are considered the primary reactors of innate immune responses [12,22]. The development of UC is always accompanied by the overactivation of macrophages. Furthermore, pyroptosis is a common form of programmed cell death for macrophages and is associated with various inflammatory diseases. Excessive amounts of cellular proinflammatory factors can leak into the extracellular space through the pore-like structures formed by the N-terminal of GSDMD (NT-GSDMD) in the cell membrane [23]. The emergence of UC was notably associated with elevated levels of IL-1β and IL-18, indicating that substances formed during pyroptosis can exacerbate colitis.

The treatment of UC remains challenging even with the emergence of established new therapies and should be precise. Targeting inflammasomes that are overly activated by the associated gut microbiota has been considered a potential therapeutic method [24]. Eugeniin is a polyphenol extracted from cloves and other plants and has a wide range of pharmacological actions. Polyphenolic compounds can protect against oxidation, cancer, inflammation, and microbial infection and have low cytotoxicity [25]. Evidence indicates that the pharmacological effects of eugeniin include inhibiting the synthesis of viral DNA, the production of nitric oxide (NO) and prostaglandin E2 (PGE2), and the activity of

histidine decarboxylase (HDC). However, the application of eugeniin to UC treatment has not been reported yet, and the underlying mechanisms remain unclear [26]. This study highlights eugeniin as an anti-inflammatory agent that targets *D. vulgaris* flagellin (DVF)-induced NAIP/NLRC4 inflammasome activation to prevent UC development. Thus, the present study will enhance the understanding of this opportunistic pathogen and offer prospective approaches for UC prevention.

Material and methods

Ethics statement

All animal experiments in this study were performed following the ethical policies and procedures approved by the ethics committee of the Tianjin Medical University, Tianjin, China (Approval no. TMUaMEC 2021017). Analysis of clinical data was performed with proper informed consent, which was reviewed and approved by The Ethical Committee of Tianjin Medical University General Hospital, Tianjin, China (Approval no. IRB2022-WZ-156).

Subjects and samples collection

Patients with clinically and histologically proven diagnosis of UC [n = 19] and controls [n = 20] were recruited from Tianjin Medical University General Hospital (Tianjin, China). Stool samples and colonic biopsies were collected after obtaining informed consent from all subjects. The two groups were age- and sex-matched and patients with other clinical diseases or a history of taking antibiotics, steroids, and probiotics were excluded. Disease activity of UC was assessed by Mayo Score, and patients with Mayo score $\geq$ 3 were considered to be at the active stage [27,28]. Likewise, fecal calprotectin concentration is a proven non-invasive biomarker to assess intestinal inflammation [29,30]. Stool samples were used to detect the abundance of *D. vulgaris*. The correlations between *D. vulgaris* and disease activity were examined using linear regression analysis. Colon biopsies were used for double immunofluorescent staining to evaluate the expression of caspase-1 and IL-18.

D. vulgaris quantification

Total microbial DNA was extracted from the feces of all subjects by using DNeasy tissue kit (Qiagen). The bacterial load in the collected fecal samples was assessed using quantitative PCR (qPCR). *D. vulgaris* quantitation was measured relative to the universal bacteria 16S. The primers of *D. vulgaris* quantification and universal bacteria 16S were shown in Table 1.

Bacterial preparation and DVF expression

D. vulgaris (ATCC 29579) was obtained from American Type Culture Collection (ATCC) and incubated anaerobically in Modified Baar's Medium (ATCC Medium1249) at 30 °C until log phase growth. The bacteria were then collected by centrifugation and resuspended in sterile phosphate-buffered saline (PBS) containing 2.5% glycerol to the final experimental concentration of 2.5×10^8 cfu/ml according to the previous studies [31] and a preliminary experiment. The recombinant DVF was expressed and purified *in vitro*. Specifically, DVF was expressed through *Escherichia coli* (*E. coli*). The coding sequence of the His-tagged DVF gene was cloned into the HindIII and BamHI restriction sites of the PSMART-I vector for its expression in *E. coli* strain BL21 (DE3). A sufficient amount of *E. coli* BL21 was subcultured in LB broth with kanamycin (50 μg/mL) at 37 °C overnight. The bacteria were harvested and lysed to collect the DVF protein.

Table 1
Primer sequences used for bacterial quantification.

Primers		Sequence
Desulfovibrio vulgaris	Forward	5′-GGCATCTGTAGACCTCCTTGTAGTC-3′
	Reverse	5′-TGTCGATCGTAGGTAGCAAATGGCG-3′
16S (universal bacteria)	Forward	5′-GCAGGCCTAACACATGCAAGTC-3′
	Reverse	5′-CTGCTGCCTCCCGTAGGAGT-3′

Animal experiments

Seven-week-old female C57BL/6 mice were purchased from the Beijing Animal Research Center, China, which were always selected as a model of dextran sulfate sodium (DSS) induced colitis with reduced differences within the groups [32]. Mice were housed in the animal center of Tianjin Medical University under a specific pathogen-free (SPF) environment with a natural light–dark cycle. All mice were acclimatized for 7 days and randomized into different groups. Mice in the DSV group were administered with an antibiotic cocktail (0.1 g/L vancomycin, 0.2 g/L ampicillin, neomycin, and metronidazole) [33,34] in drinking water for 3 days and 5×10^7 cfu *D. vulgaris* for 7 days. Mice in the DVF group were gavaged 2 μg of DVF daily for 10 days, and sterile PBS was used as control.

Eugeniin (CAS: 58970–75-5, purity > 98.0%) was obtained from Chengdu Push Bio-Technology Co., Ltd. 32 remaining mice were randomized into 4 groups: PBS, Eugeniin, DVF, and Eugeniin with DVF groups. Eugeniin was dissolved in PBS and administered to mice at 40 mg/kg daily for 10 days according to the previous studies and preliminary experiment [35]. The mice were also given 3% DSS dissolved in sterile drinking water for 7 days to establish a DSS-induced colitis model. The mice were sacrificed, and the colons and spleens were harvested for analyses. Body weight and disease activity index (DAI) were measured daily during the experimental period.

Reverse transcription and real-time quantitative PCR

Total RNA from tissues or cell lines was homogenized and isolated using TRIzol Reagent (Ambion, cat #15596026). Reverse transcription of cDNA was performed with TIANScript RT Kit (TIANGEN, China). Real-time PCR analysis was carried out using the extracted cDNA as templates as well as TaqMan Gene Expression Master Mix (Genewiz, China) and primers. Each sample underwent three independent tests. Glyceraldehyde-3-phosphate dehydrogenase (GAPDH) was selected as endogenous control. The expression of each target gene was determined by $2^{-\Delta\Delta CT}$ method. The oligonucleotide primers are presented in Table 2.

Western blot analysis

The colon tissues or cell lines were disintegrated with cold RIPA buffer (Beyotime.P0013B) supplemented with protease inhibitors (Solarbio, China) on ice for 10 min. The supernatant was collected after adequate homogenization and centrifugation. The proteins were loaded onto an SDS-polyacrylamide gel electrophoresis system with 8 μL of the initial protein amount. The exact amount for different groups was adjusted according to the internal control. The size-separated proteins were blotted onto polyvinylidene fluoride (PVDF) membranes (Invitrogen, USA). After blocking with 10% bovine serum albumin, the membranes were cut into bands and incubated with primary anti-α-tubulin antibody (1:1000, #2125,

Table 2
Primer sequences used for Realtime-PCR.

Primers		Sequence
mGAPDH	Forward	5′-GGAGAAACCTGCCAAGTATG-3′
	Reverse	5′-TGGGAGTTGCTGTTGAAGTC-3′
mIL-1β	Forward	5′-ACGGACCCCAAAAGATGAAG-3′
	Reverse	5′-TTCTCCACAGCCACAATGAG-3′
mIL-18	Forward	5′-GCCTCAAACCTTCCAAATCAC-3′
	Reverse	5′-GTTGTCTGATTCCAGGTCTCC-3′
mCaspase1	Forward	5′-CTTGGAGACATCCTGTCAGGG-3′
	Reverse	5′-AGTCACAAGACCAGGCATATTCT-3′
hGAPDH	Forward	5′-GGAGAAACCTGCCAAGTATG-3′
	Reverse	5′-TGGGAGTTGCTGTTGAAGTC-3′
hIL-1β	Forward	5′-ATGCACCTGTACGATCACTG-3′
	Reverse	5′-ATGCACCTGTACGATCACTG-3′
hIL-18	Forward	5′-CACCCCGGACCATATTTATT-3′
	Reverse	5′-TCATGTCCTGGGACACTTCTC-3′

Cell Signaling Technology), anti-IL-1β antibody (1:1000, #12242, Cell Signaling Technology), anti-IL-18 antibody (1:1000, ab71495, Abcam), anti-caspase1 antibody (1:1000, ab179515, Abcam), anti-NLRC4 antibody (1:1000, ab201792, Abcam) or anti-GSDMD antibody (1:1000, ab209845, Abcam) overnight at 4 °C. On the following day, the bands were incubated with HRP-linked anti-mouse IgG (1:5000, Cell Signaling Technology) or HRP-linked anti-rabbit (1:5000, Cell Signaling Technology) for 1 h at room temperature. The immuno-reactive bands were detected by enhanced chemiluminescence and analyzed by Image J software (Image J 1.52).

Double immunofluorescent staining

The colonic tissues of mice or patients were fixed with 4% formaldehyde solution and then embedded with paraffin. Samples were segmented into slices and blocked with 0.3% bovine serum albumin for 1 h at room temperature. The sections were incubated with the following primary antibodies: rat anti-IL-18 antibody (1:100, ab71495, Abcam), rabbit anti-cleaved-caspase-1 antibody (1:100, #89332, Cell Signaling Technology), or rabbit anti-IL-1β antibody (1:100, a16288, Abclonal) at 4 °C overnight. Meanwhile, the macrophages were labeled by F4/80 in mice and CD68 in human [36]. After washing with PBST, the slides were mounted with 40,6-diamidino-2-phenylindole (DAPI). Images were viewed and taken by fluorescent microscope (Lycra, Germany).

Cell cultures and treatments

The rat macrophage-like cell line RAW 264.7 was obtained from the American Type Culture Collection (ATCC, Manassas, VA, USA) and cultured in Dulbecco's Minimum Essential Medium supplemented with 10% FBS (Gibco, Life Technologies) in a humidified atmosphere with 5% CO_2 at 37 °C. The human monocyte line THP-1 was purchased from ATCC and cultured in RPMI 1640 medium containing 10% FBS. THP-1 cells were treated with 100 nM phorbol 12-myristate 13-acetate (PMA) for 24 h to differentiate into macrophage-like cells [37,38]. The cells were seeded in 12-well plates and treated with PBS, DVF, Lipofectamine 3000 (Invitrogen, USA), or DVF transfected with Lipofectamine 3000 for 24 h [39]. Eugeniin was dissolved in PBS, and the concentration for cell treatments was 25 μM according to the preliminary experiment [26]. The expression levels of mRNA and protein were measured after the application of different interventions.

Transfection of NLRC4 short hairpin (sh) RNA

RAW 264.7 cells were added into 12-well plates and transfected with the NLRC4 shRNA plasmids by Lipofectamine 3000 in Opti-MEM I medium for 6 h following the manufacturer's instructions. The target sequence was GCG ATG ACC TCT TTG CAT TGA (GenePharma, China) and the shRNA plasmid targeted scrambled sequence was used as a negative control. Subsequently, the transfected cells were treated with lipo3000 or DVF with lipo3000 for 24 h. The transfection effect and the expression of the related proteins were assessed by Western blot analysis.

RNA sequencing

Following the extraction of the qualified RNA samples from RAW 264.7 cells, mRNA was enriched with oligo (dT) beads. The mRNA was fragmented to synthesize cDNA, which was initially quantified by Qubit 2.0 and sequenced on HiSeq X-Ten (Illumina). Data were filtered by NGS QC Toolkit (v2.3.3) after sequencing and aligned using TopHat (v2.0.13) [40]. Gene expression was normalized using the expected number of fragments per kilobase of transcript per million mapped reads (FPKM). Differentially expressed genes were analyzed using the Noiseq software package. The functional classification annotation and functional significance enrichment of differentially expressed genes were analyzed.

LDH release assay

The lactate dehydrogenase (LDH) assay kit (Jiancheng Bio, Nanjing, China) was used to assess LDH released in the culture medium of RAW264.7 cells. After different stimulation methods, the cell culture supernatant was collected and centrifuged at 850 g for 3 min, and the cell debris was discarded. The supernatant was mixed with the LDH working solution added to 96-well plates and incubated at 37 °C for 30 min based on the description of the reagents. Optical density (OD) was measured at the wavelength of 450 nm with a microplate reader.

Calcein-AM/propidium iodide (PI) staining assay

Calcein-AM/PI double stain kit (Solarbio, Beijing) was applied to quantify the number of living and dead cells. After different stimulation, THP-1 cells in 12-well plates were washed and stained with 2 μM calcein-AM and 1.5 μM PI mixed with 1 × assay buffer per well at 37 °C for 30 min. The cells were photographed immediately by fluorescent microscope. Live cells were green and dead cells were red as detected by different excitation filters. The number of PI positive cells was computed by the equation: PI positive cells (%) = (PI positive cells/total cells) × 100, and represented pyroptosis.

Transmission electron microscopy (TEM)

After different stimulation, RAW264.7 cells were centrifuged and collected. The cell pellets were fixed with 2.5% glutaraldehyde (EM Grade, Solarbio) and then dehydrated in a graded series of ethanol concentrations. All samples were embedded using pure acetone and an embedding solution (EPON812). The ultrathin sections were divided into 70 nm slices and double-stained with 2% uranyl acetate-lead citrate [41]. Images were acquired by transmission electron microscope HT7800 (Hitachi, Japan).

Protein-protein docking and high-throughput screening

The entry ID of NAIP was Q13075 · BIRC1_HUMAN obtained from UniProt (https://www.uniprot.org/). The crystal structure of NAIP was downloaded from Protein Data Bank (PDB, https://www.rcsb.org), and the three-dimensional protein structure of DVF was created by MODELLER (https://salilab.org/modeller/) based on the amino acid sequence. Subsequently, the initial struc-

tures were subjected to hydrogenation, hydrogen bond optimization, and steric hindrance optimization to minimize the stereoscopic conflict until the root-mean-square deviation (RMSD) reached a maximum cutoff of 0.3 Å [42]. NAIP acted as a receptor while DVF acted as a ligand. Two proteins were docked by HEX software under the selected docking parameters. The Hex SPF algorithm has been validated for protein–protein docking in CAPRI (Critical Assessment of Predicted Interactions) blind docking experiment. The docking proceeds by rotating the receptor and ligand about their centroids at each of a range of intermolecular distances. According to the docking structure of the DVF/NAIP complex, the protein interaction interface was set as an active pocket to high-throughput screen the inhibitors from Traditional Chinese medicine (TCM) databases. In addition, the energy of three-dimensional structures was minimized using the Optimized Potentials for Liquid Simulations (OPLS)-2005 force field and three-dimensional structures of TCM monomers were generated by LigPrep.

Statistical analysis

GraphPad Prism (GraphPad Software, Inc., USA) and SPSS 24.0 (SPSS, Chicago, Illinois, United States) were applied for all statistical analyses. The data of the biological experiments conducted in triplicate were represented by error bar and expressed as mean ± SEM. We applied two-tailed unpaired Student's *t*-test for the analysis of two groups and used one-way analysis of variance (ANOVA) for the statistics of multiple groups. P value < 0.05 was determined as statistically significant.

Results

D. vulgaris was enriched in patients with UC

To investigate the pathogenic role of *D. vulgaris* in UC development, we detected its abundance in patients with UC and healthy controls (HC). The qPCR data showed that *D. vulgaris* was more enriched in the feces of patients with UC (Fig. 1A), and its abundance was positively correlated with some indicators of UC activity, including Mayo score (r = 0.4589, p = 0.0481) and fecal calprotectin levels (r = 0.5874, p = 0.0272) (Fig. 1B-C). Furthermore, the occurrence of macrophage pyroptosis in colon tissues was examined using double immunofluorescent staining. Inflammasome-associated inflammatory caspases including caspase-1 induced cleavage of GSDMD and then resulted in the maturation of IL-1β and IL-18, which was required and sufficient for pyroptosis. The expression of caspase-1 and IL-18 was upregulated in the inflamed mucosa of patients with UC compared with the controls in $CD68^+$ macrophages (Fig. 1D). Hence, enriched *D. vulgaris* in the human gut and overactivated macrophage pyroptosis may play a potential role in UC development.

D. vulgaris or its flagellin facilitated DSS-induced colitis in mice

Whether *D. vulgaris* can promote colitis and by which components interact with the host need to be further investigated. Bacterial flagellin is a potential activator of the immune system and causes inflammatory disorders [43]. Therefore, we investigated whether flagellin is one of the vital pathogenic elements of DSV. The effects of *D. vulgaris* or its recombinant flagellin on DSS-induced colitis in mice were assessed (Fig. 2A). Compared with the PBS group, the gavage of DSV or DVF significantly increased the intestinal inflammation under the induction of DSS, as demonstrated by more severe body weight loss and higher disease activity index (DAI) score (Fig. 2B-C). No significant difference was observed among groups administered with normal drinking water without DSS. The colons were significantly shorter after treatment with DSV or DVF with DSS (Fig. 2D-E). In addition, we have observed an increase in spleen weight, which is proportional to the severity of colitis inflammation (Fig. 2F). Histological analysis also indicated that mice treated with DSV or DVF showed remarkable exacerbation of mucosal damage, inflammatory cell infiltration, and crypt loss (Fig. 2G). These results indicated the proinflammatory effect of *D. vulgaris* or its flagellin on DSS-induced colitis.

D. vulgaris or DVF induced pyroptosis of intestinal macrophages in mice

We further explored the occurrence of macrophage pyroptosis after treatment with DSV or DVF to investigate the proinflammatory mechanism. The expression of cleaved caspase-1 (c-caspase-1), which acts as a 'scissors' protein during pyroptosis, increased in $F4/80^+$ macrophages in the inflamed mucosa lamina propria (Fig. 3A). The terminal cytokine IL-1β was elevated predominantly in $F4/80^+$ macrophages, but not in intestinal epithelial cells, as evident in the mucosal biopsy results of the DSV and DVF groups (Fig. 3B). The result of pyroptosis is the release of intracellular proinflammatory cytokines to activate an inflammatory response. The transcript levels of IL-1β and IL-18 increased in mice treated with DSV or DVF compared with those of controls (Fig. 3C). These findings were confirmed by the Western blot analysis, indicating the upregulation of c-caspase-1, NT-GSDMD, and cleaved cytokines IL-1β and IL-18 (Fig. 3D). Therefore, DVF-induced macrophage pyroptosis plays a crucial role in this process.

DVF facilitated inflammation by inducing macrophage pyroptosis in vitro

To further detect the role of macrophages and the mechanism of DVF-induced proinflammatory effect, we investigated the expression of genes related to pyroptosis *in vitro*. Interestingly, the direct stimulation by DVF did not upregulate the expression of genes associated with pyroptosis and inflammation. However, when delivering the DVF to the cytoplasm through lipo3000, the relative mRNA levels of caspase-1, IL-1β, and IL-18 significantly increased in RAW264.7 or THP-1 cells (Fig. S1C and S1E). RNA sequencing was performed on RAW264.7 cells from the lipo3000 or DVF with lipo3000 group. The volcano plots indicated the different expression levels of the two groups (Fig. S1A). Analysis of the GO database showed that differentially expressed genes were mainly involved in immune system process, inflammatory response, positive regulation of cytokine production, and positive regulation of defense to the bacterium (Fig. 4A). The genes associated with pyroptosis between the two groups were displayed in the heatmap, which showed the up-regulated expression in the DVF group (Fig. 4B). Based on the KEGG analysis, DVF significantly upregulated the genes involved in the cytokine-cytokine receptor signaling pathway, NLR signaling pathway, and IBD (Fig. S1B). The Western blot showed that the protein levels of c-caspase-1, NT-GSDMD, and cytokines IL-1β and IL-18 were upregulated (Fig. 4C). Furthermore, the occurrence of pyroptosis is generally accompanied by the release of cytoplasmic lactate dehydrogenase (LDH), which increased in the cell supernatant of the DVF with lipo3000 group (Fig. S1D). In addition, cellular morphology was observed through light microscopy. The DVF transfected by lipo3000 induced obvious pyroptosis in THP-1 cells, leading to cell swelling, nucleus concentration, and cystoid formation (Fig. 4D). Calcein-AM/PI double staining showed that DVF with lipo3000 increased the cell pyroptosis, which was characterized by a higher density of PI staining

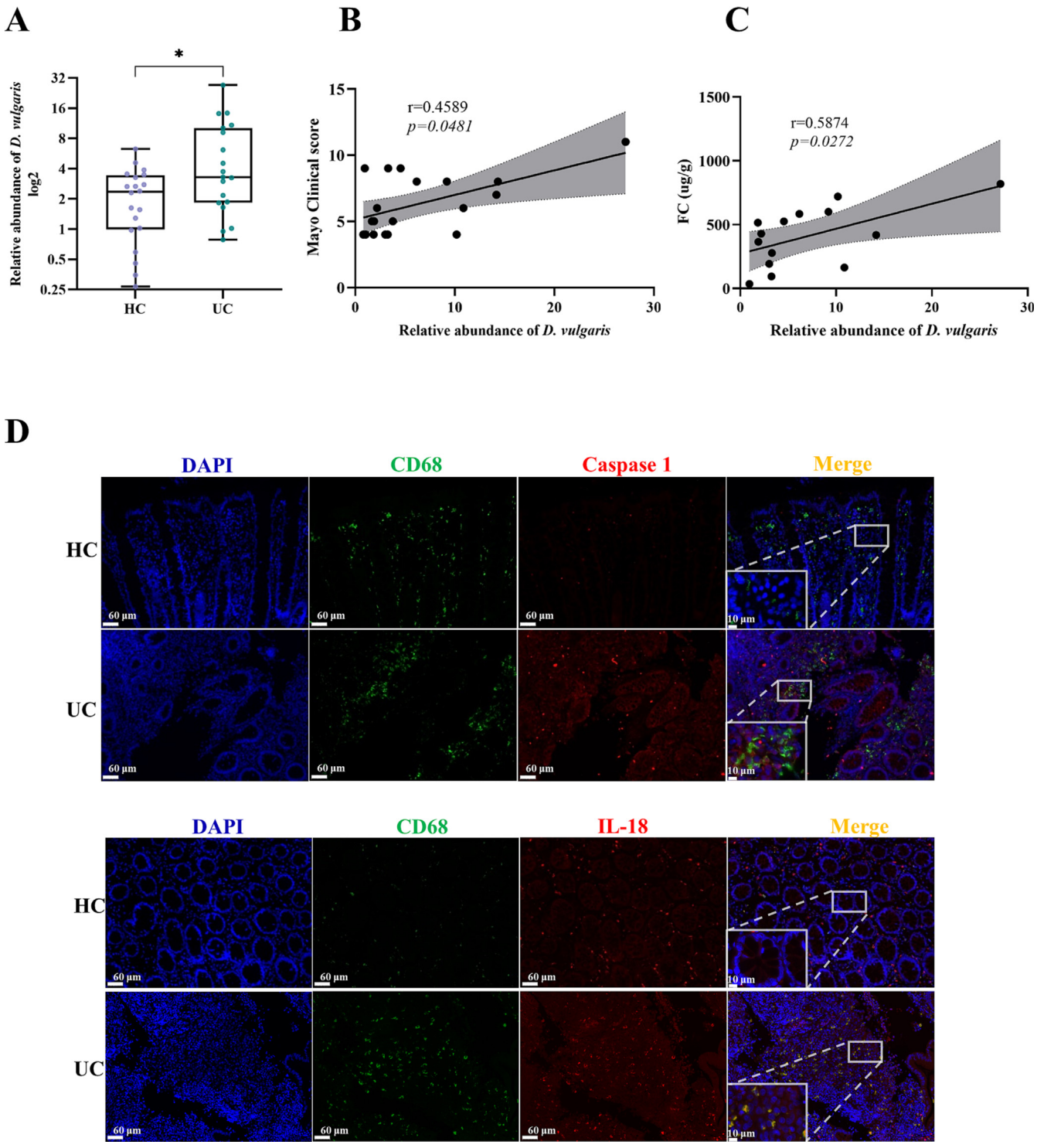

Fig. 1. The abundance of *D. vulgaris* was increased in the feces of patients with UC and related to disease severity. (A) The relative abundance of *D. vulgaris* in feces from UC (n = 19) and HC (n = 20). (B) Correlation analysis between the relative abundance of *D. vulgaris* and Mayo clinical score (n = 19). (C) Correlation analysis between the relative abundance of *D. vulgaris* and FC in patients with UC (n = 14). (D) Immunofluorescent images of human colon tissues stained for cell nucleus (blue), CD68 (green), caspase1 or IL-18 (red) and merge. Scale bars, 10 μm or 60 μm. *D. vulgaris*, *Desulfovibrio vulgaris*; HC, healthy controls; UC, ulcerative colitis; FC, fecal levels of calprotectin. *p < 0.05. (For interpretation of the references to colour in this figure legend, the reader is referred to the web version of this article.)

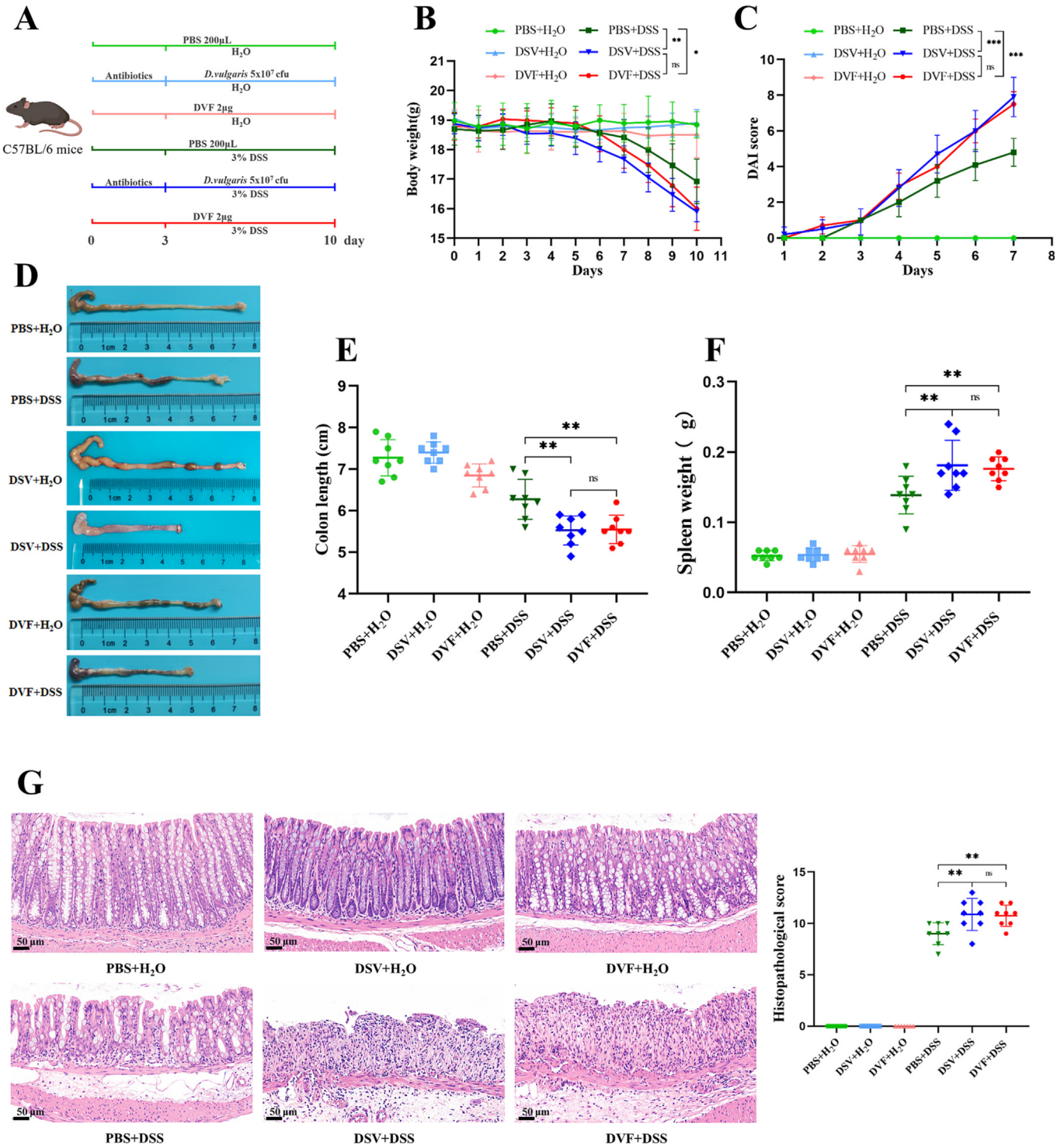

Fig. 2. *D. vulgaris* or its flagellin facilitated DSS-induced colitis in mice. (A) Schematic illustrating the experimental procedure of DSS-induced colitis. (B-C) Changes in body weight(B) and DAI score(C) of mice. (D) Representative images of the colon. (E-F) Changes of colon length(E) and spleen weight(F) in mice of different groups were analyzed. (G) Representative histological images of H&E-stained colon tissues (left panel) and colon histopathological score (right panel). Scale bars, 50 μm. PBS, phosphate-buffered saline; *D. vulgaris* (DSV), *Desulfovibrio vulgaris*; DVF, *Desulfovibrio vulgaris* flagellin; DAI, disease activity index; DSS, dextran sulfate sodium. $^{*}p < 0.05$, $^{**}p < 0.01$, $^{***}p < 0.001$. *ns*, not significant.

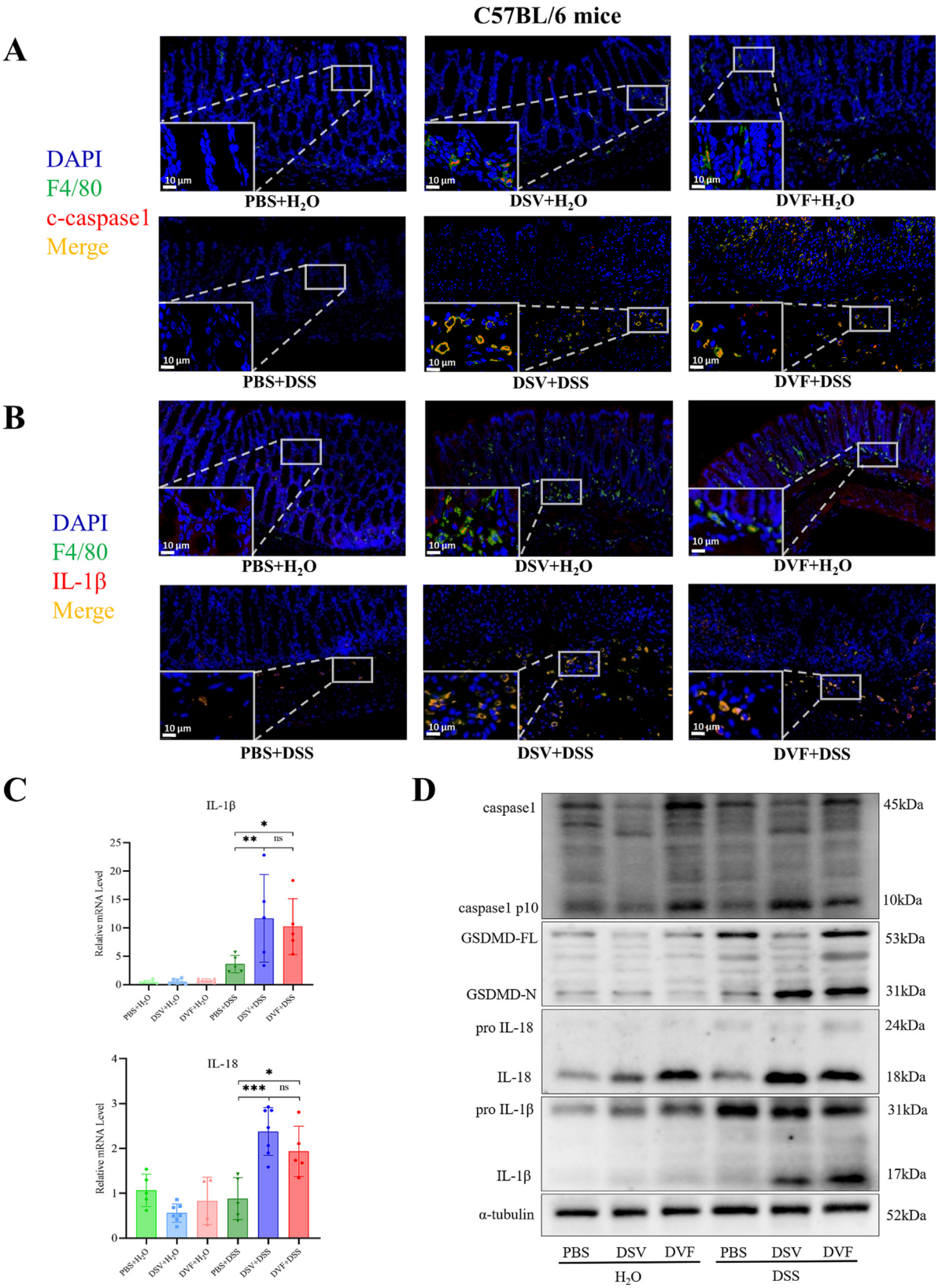

Fig. 3. *D. vulgaris* or DVF induced pyroptosis of intestinal macrophages in mice. (A) Immunofluorescent images of mice colon tissues stained for cell nucleus (blue), F4/80 (green), cleaved-caspase1 (red) and merge. (B) Immunofluorescent images of mice colon tissue stained for cell nucleus (blue), F4/80 (green), IL-1β (red) and merge. (C) Relative mRNA expression levels of IL-1β and IL-18 in the colon. (D) The protein levels of caspase1, GSDMD, IL-18, and IL-1β in pyroptosis pathway were measured by western blotting. Scale bars, 10 μm. c-caspase1, cleaved-caspase1; *D. vulgaris* (DSV), *Desulfovibrio vulgaris*; DVF, *Desulfovibrio vulgaris* flagellin; GSDMD, gasdermin D; PBS, phosphate-buffered saline. $^{*}p < 0.05$, $^{**}p < 0.01$, $^{***}p < 0.001$. *ns*, not significant. (For interpretation of the references to colour in this figure legend, the reader is referred to the web version of this article.)

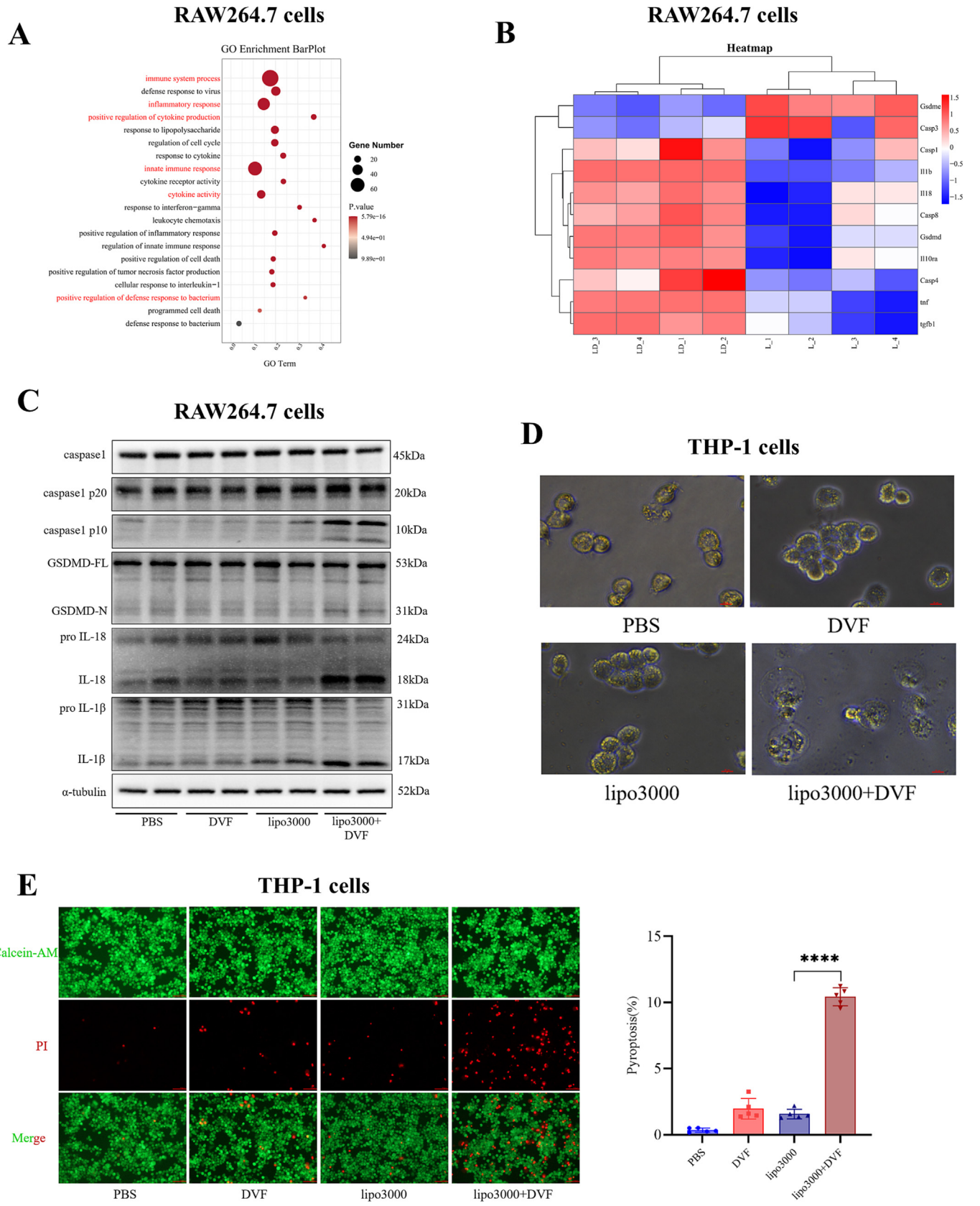

Fig. 4. DVF induced pyroptosis of macrophages *in vitro*. (A) GO analysis of genes significantly upregulated in DVF with lipo3000 treated macrophages. (B) Heatmap of RNA-seq from the lipo3000 group and lipo3000 with DVF group. (C) The protein levels of indicators in the pyroptosis pathway were measured by western blotting. (D) Representative light microscope images of THP-1 cells. Scale bars, 10 μm. (E) Images of THP-1 cells stained for Calcein-AM (green), PI (red), and merge. Scale bars, 100 μm. DVF, *Desulfovibrio vulgaris* flagellin; PBS, phosphate-buffered saline; GO, gene ontology; GSDMD, gasdermin D; PI, propidium Iodide; ****$p < 0.0001$. (For interpretation of the references to colour in this figure legend, the reader is referred to the web version of this article.)

(Fig. 4E). These findings indicated that DVF induced macrophage pyroptosis *in vitro*, which further lead to proinflammatory effects.

DVF induced macrophage pyroptosis via NAIP/NLRC4 inflammasome, which could be inhibited by eugeniin

NAIP/NLRC4 inflammasome, as an intracellular receptor for flagellin, may play a vital role in DVF-induced pyroptosis. We knocked down the expression of NLRC4 in RAW264.7 cells, and found that the activation of caspase-1 and cell pyroptosis caused by DVF were blocked. These results indicated that DVF-induced macrophage pyroptosis was largely dependent on NAIP/NLRC4 inflammasome (Fig. 5A). Therefore, targeting the interaction between DVF and NAIP could be a treatment modality for colitis. In this regard, we further evaluated their potential interaction through protein–protein docking. The docking results showed that four hydrogen bond interactions were formed between NAIP and DVF. The amino acids involved in the interfacial interaction were formed by Ser691, Asp718, Ala713, and Glu714 of NAIP and Gln249, Ser250, Glu246, and Ser239 of DVF (Fig. 5B and S2A). Based on the structure of the DVF/NAIP complex obtained from docking, the binding site was set as an active pocket to select the lead compound from the TCM database. The compounds with the highest docking score were shown in Fig. 5C, eugeniin ranked first as the most effective blocker for the interaction between DVF and NAIP. The binding mode of eugeniin and the DVF/NAIP complex was determined by molecular docking simulation. Eugeniin blocked the interaction in the DVF/NAIP complex by binding with Glu706, Ser702, Lys698, and Glu714 of NAIP and Asn236, Ser239, and Asn240 of DVF (Fig. 5D and S2B). We further evaluated the role of eugeniin in DVF-induced macrophage pyroptosis by electron microscopy, and found that it inhibited pore formation and cell disruption (Fig. 5E and S2C). The protein levels of c-caspase-1, GSDMD, IL-1β, and IL-18, which play pivotal roles in pyroptosis, significantly decreased after the eugeniin treatment compared with those in the DVF group (Fig. 5F). These findings suggest the direct action between DVF and NAIP at the molecular level and the potential blocking effect of eugeniin.

Eugeniin therapy rescued the DVF-induced proinflammatory effect in mice

The role of eugeniin in attenuating the experimental colitis was further assessed in mice (Fig. 6A). The protective effect of eugeniin was not significant compared with that in the PBS group but rescued the DVF-induced proinflammatory effect. Eugeniin led to the remission of colon inflammation as indicated by the lower body weight loss and DAI score than those in the DVF group (Fig. 6-B-C). Treatment with eugeniin significantly increased the length of the colons and decreased the spleen weights (Fig. 6D-F). Eugeniin rescued the intestinal inflammation induced by DVF according to the histological analysis (Fig. 6G). The levels of c-caspase-1 and IL-1β decreased in F4/80^{+} macrophages, suggesting the effectiveness of eugeniin in targeting DVF-induced NAIP/NLRC4 inflammasome activation and pyroptosis (Fig. S2A-B). The gene expression levels of IL-1β and IL-18 decreased in the DVF and eugeniin groups (Fig. 6H). The Western blot analysis also demonstrated the role of eugeniin in blocking pyroptosis caused by DVF (Fig. 6I).

Discussion

The balance of interactions between the gut microbiota and host immune systems plays an indispensable role in maintaining intestinal homeostasis. Previous studies suggested that *Desulfovibrionaceae* was enriched in patients with IBD [44]. We consistently found that the relative abundance of *D. vulgaris* increased in the feces of patients with UC and was associated with disease activity. This finding may reveal the potential role of DSV in the development of UC. However, the bacterial pathogenic components and the underlying mechanisms remain unclear. DSV has a flagellum that is involved in bacterial motility, colonization, and adhesion to the host. Flagellin is essential for innate immune detection in the gut, but may impair the innate immunity to promote the development of intestinal inflammation [45]. Thus, new targets should be identified to regulate disorders related to microbiota-host interaction. In the present study, we investigated the proinflammatory effect of DSV and its flagellin, which were demonstrated to significantly aggravate experimental colitis in mice. Hence, DSV might be a potential proinflammatory bacterium in the gut and its flagellin played a crucial role in the process. However, to what extent the proinflammatory effect of DSV depends on its flagellin and other bacterial components or metabolites need further study.

As a group of multiprotein complexes in the cytoplasm that mediates cell pyroptosis and induces mature IL-1β and IL-18 production, the inflammasome has a controversial role in IBD development [20,46,47]. Multiple Gram-negative bacteria were largely overgrown and exacerbated the pathology of colitis, such as [48]. We found that *D. vulgaris* and DVF could induce intestinal inflammation in mice, and the immunofluorescent staining showed that pyroptosis mainly occurred in macrophages. In addition, we also discovered that the expressions of caspase-1, IL-1β and IL-18 were increased in the DSV and DVF groups, suggesting that *D. vulgaris* and DVF induced pyroptosis of macrophages could be mediated by caspase-1. Recent studies have revealed that caspase-1-mediated pyroptosis is a proinflammatory form of programmed cell death in macrophages. It releases an excess of cytokines and triggers a series of responses in surrounding cells [49]. Excessive production of IL-1β and IL-18 is correlated with intestinal injury and colitis development [21]. Thus, intestinal macrophages are of great necessity to respond to bacterial challenges, but overreaction can lead to the dysregulation of immunity and inflammation. Gasdermin D, encoded by GSDMD on chromosome 8 (8q24.3), is a protein made of a 31 kDa N-terminus (GSDMD-N) and a 22 kDa C-terminus (GSDMD-C) connected by a peptide linker [50]. GSDMD was initially found in the homologues of GSDMA [51] and was widely expressed in different tissues and immune cells [52]. Upon activation, the linker is cleaved to separate GSDMD-N from its autoinhibitory domain, GSDMD-C [53]. GSDMD is a generic substrate for caspase-1. Crystal structure of caspase-1-GSDMD-C complex showed a similar GSDMD-recognition mode. Cleavage of GSDMD by the inflammatory caspases critically determined pyroptosis by releasing the cleaved GSDMD-N domain that bears intrinsic pyroptosis-inducing activity [54]. However, a variety of bacterial components and stimuli could trigger multiple types of inflammasome to mediate pyroptosis. For example, it has been found that XBP1 deficiency promoted the extracellular release of mitochondrial DNA by activating NOD-like receptor pyrin domain containing 3 (NLRP3)/caspase-1/GSDMD signaling, which increased the production of ROS and promoted pyroptosis [55]. During macrophage apoptosis, NLRP3 inflammasome induces caspase-8/-3 to cut Gasdermin E and release IL-1β, thus promoting inflammation [56]. Thus, whether DVF can promote other types of cell death through another inflammasome and whether caspase-1/GSDMD is the main mediator in this process is worth further exploration.

Among the NLR family, NLRC4 has been widely studied and has an important role in the defense of cytoplasmic PAMPs including flagellin. Meanwhile, NLRP3 inflammasome is always activated by pathogens, microbial toxins, nucleic acids, ATP, and crystalline substances [57]. To further verify the effect of DVF on inflammasome activation in macrophages, we treated RAW264.7 and

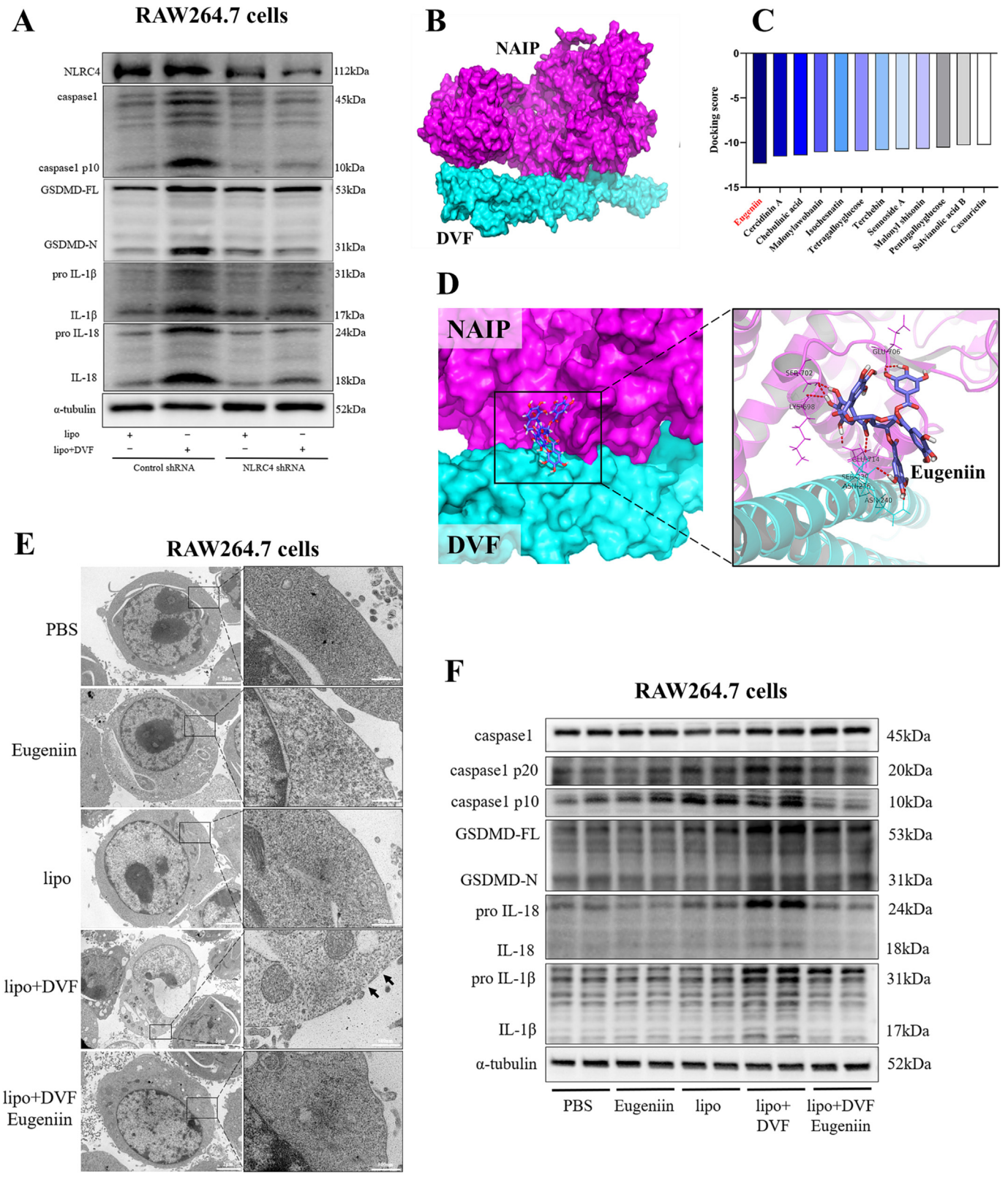

Fig. 5. DVF induced macrophage pyroptosis via NAIP/NLRC4 inflammasome activation, which could be inhibited by eugeniin. (A) The protein levels of pyroptosis indicators in macrophages transfected with NLRC4 shRNA were measured by western blotting. (B) Protein-protein docking of DVF and NAIP. (C) Molecular docking results of high-throughput screening in terms of the structure of DVF/NAIP complex. (D) Predicted binding modes of eugeniin and DVF/NAIP complex and its three-dimensional structure. (E) Representative transmission electron microscope images of RAW264.7 cells. Scale bars, 2 μm, 5 μm, or 500 nm. (F) The protein levels in the pyroptosis pathway were measured by western blotting after eugeniin treatment. DVF, *Desulfovibrio vulgaris* flagellin; shRNA, short hairpin RNA; NAIP, NLR family of apoptosis inhibitory protein; GSDMD, gasdermin D; PBS, phosphate-buffered saline; lipo, Lipofectamine 3000.

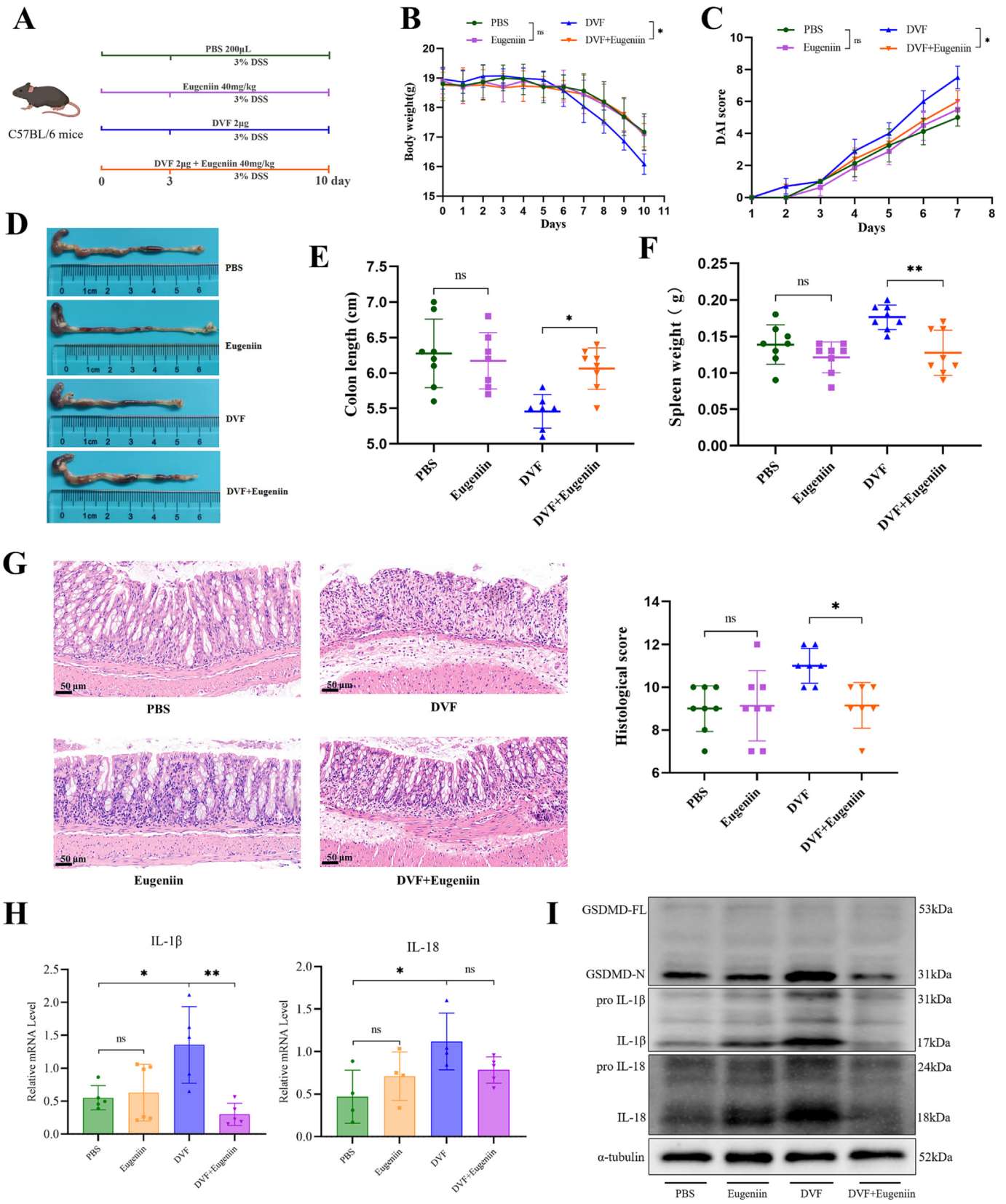

Fig. 6. Eugeniin treatment alleviated the DVF-induced proinflammatory effect in mice. (A) Schematic illustration of the experimental procedure. (B-C) Changes of body weight(B) and DAI score(C) in mice. (D) Representative images of the colon. (E-F) Changes in colon length(E) and spleen weight(F) in different groups were analyzed. (G) Representative histological images of colon tissues stained with H&E (left panel) and the histopathological score of colon inflammation (right panel). (H) Relative mRNA expression levels of IL-1β and IL-18 in the colon. (I) The protein levels of indicators in pyroptosis pathway were measured by western blotting. Scale bars, 50 μm. PBS, phosphate-buffered saline; DVF, *Desulfovibrio vulgaris* flagellin; DSS, dextran sulfate sodium; DAI, disease activity index; GSDMD, gasdermin D, $^{*}p < 0.05$, $^{**}p < 0.01$, $^{****}p < 0.0001$. *ns*, not significant.

THP-1 cells with DVF *in vitro*. DVF did not induce pyroptosis directly but strongly triggered inflammatory responses after transfection into the cytoplasm by lipo3000. These results suggest that the receptors in the cell cytoplasm might have a crucial effect on this effect. Apoptosis-associated speck-like protein containing CARD (ASC), which bridges pro-caspase-1 and pyrin-containing receptors, is indispensable in the assembly of most inflammasomes. However, NLRC4 inflammasome was unique because they directly interact with pro-caspase-1 without ASC. RAW264.7 cells were naturally ASC-deficient and could activate NAIP/NLRC4 inflammasome. Meanwhile, when NLRC4 was knocked down, the activation of caspase-1 and pyroptosis induced by DVF was blocked. Taken together, our findings suggest that NAIP/NLRC4 inflammasome may be the primary responder to DVF, consistent with previous results demonstrating that NAIP/NLRC4 inflammasome complex is a sensor of intracellular flagellin. Therefore, inhibiting DVF-induced macrophage pyroptosis and its consequent exaggerated cytokine release might be an effective strategy to reduce inflammation.

UC is a persistent intractable inflammatory disorder that urgently needs new and effective therapeutic agents. The application of currently available drugs has problems, such as low efficiency, serious adverse reactions and resistance. Therefore, traditional Chinese medicine has gradually attracted wide attention because it had few side effects and reduced intestinal disorders. In this study, we screened lead compounds by high-throughput molecular docking in the TCM database. We speculate that eugeniin could be the most effective DVF/NAIP interaction interface inhibitor. Recent studies suggest that eugeniin possesses antioxidant and antiviral properties [58,59]. As such, we investigated its role in blocking the DVF/NAIP interaction, leading to suppressed caspase-1 activity and reduced GSDMD cleavage to inhibit macrophage pyroptosis. However, eugeniin alone has not shown a beneficial or harmful effect on intestinal inflammation. Our results suggest that eugeniin inhibited DVF-induced inflammation, and could provide a new target for the precise treatment of UC. Nevertheless, the safety, specificity, and persistence of eugeniin in the treatment of UC remain to be discussed.

In summary, we found that *D. vulgaris* and DVF could induce intestinal inflammation via NAIP/NLRC4 inflammasome activation and macrophage pyroptosis, which could be targeted by eugeniin. This study may provide a novel mechanism for *D. vulgaris*-mediated colitis and a promising target for UC therapy.

Conclusion

D. vulgaris was overgrown in patients with UC. *D. vulgaris* or its flagellin could facilitate DSS-induced colitis via NAIP/NLRC4 inflammasome activation and macrophage pyroptosis. Targeting the interfaces of DVF and NAIP by eugeniin inhibits the proinflammatory effect induced by DVF, but eugeniin alone did not show beneficial effects on colitis. Our study emphasizes the significance of the gut microbiota as a crucial modulator of the human innate immune system and might open up novel therapeutic avenues for UC treatment.

Compliance with Ethics Requirements

All Institutional and National Guidelines for the care and use of animals (fisheries) were followed.

All experiments involving animals were conducted according to the ethical policies and procedures approved by the ethics committee of the Tianjin Medical University, Tianjin, China (Approval no. TMUaMEC 2021017).

Analysis of clinical data was performed with proper informed consent, which was reviewed and approved by The Ethical Committee of Tianjin Medical University General Hospital, Tianjin, China (Approval no. IRB2022-WZ-156).

CRediT authorship contribution statement

Yaping An: Methodology, Data curation, Writing – original draft, Investigation, Software, Validation, Writing – review & editing. **Zihan Zhai:** Data curation, Writing – original draft, Software, Validation. **Xin Wang:** Data curation, Visualization, Investigation, Software, Validation, Writing – review & editing. **Yiyun Ding:** Data curation, Writing – original draft, Investigation, Software, Validation. **Linlin He:** Investigation, Software, Validation. **Lingfeng Li:** Visualization, Investigation. **Qi Mo:** Software, Writing – review & editing. **Chenlu Mu:** Investigation, Software. **Runxiang Xie:** Methodology, Validation. **Tianyu Liu:** Investigation, Visualization. **Weilong Zhong:** Validation, Data curation. **Bangmao Wang:** Validation, Data curation, Supervision, Project administration, Funding acquisition. **Hailong Cao:** Conceptualization, Methodology, Investigation, Validation, Data curation, Supervision, Project administration, Funding acquisition.

Declaration of Competing Interest

The authors declare that they have no known competing financial interests or personal relationships that could have appeared to influence the work reported in this paper.

Acknowledgements

This study was supported by National Natural Science Foundation of China [grant numbers 82270574, 82070545, 82170558, 82000511, 82100574] and Key Project of Science and Technology Pillar Program of Tianjin [grant number 20YFZCSY00020].

Appendix A. Supplementary material

Supplementary data to this article can be found online at https://doi.org/10.1016/j.jare.2023.08.008.

References

[1] Krugliak Cleveland N, Torres J, Rubin DT. What Does Disease Progression Look Like in Ulcerative Colitis, and How Might It Be Prevented. Gastroenterology 2022;162(5):1396–408.
[2] Kobayashi T, Siegmund B, Le Berre C, et al. Ulcerative colitis. Nat Rev Dis Primers 2020;6(1):74.
[3] Yuan X, Chen B, Duan Z, et al. Depression and anxiety in patients with active ulcerative colitis: crosstalk of gut microbiota, metabolomics and proteomics. Gut Microbes 2021;13(1):1987779.
[4] van de Guchte M, Mondot S, Doré J. Dynamic Properties of the Intestinal Ecosystem Call for Combination Therapies, Targeting Inflammation and Microbiota. Ulcerative Colitis Gastroenterol 2021;161(6):1969–1981.e12.
[5] Barberio B, Facchin S, Patuzzi I, et al. A specific microbiota signature is associated to various degrees of ulcerative colitis as assessed by a machine learning approach. Gut Microbes 2022;14(1):2028366.
[6] Singh SB, Coffman CN, Carroll-Portillo A, Varga MG, Lin HC. Notch Signaling Pathway Is Activated by Sulfate Reducing Bacteria. Front Cell Infect Microbiol 2021;11:695299.
[7] Lennon G, Balfe Á, Bambury N, et al. Correlations between colonic crypt mucin chemotype, inflammatory grade and Desulfovibrio species in ulcerative colitis. Colorectal Dis 2014;16(5):O161–9.
[8] Rowan F, Docherty NG, Murphy M, et al. Desulfovibrio bacterial species are increased in ulcerative colitis. Dis Colon Rectum 2010;53(11):1530–6.
[9] Figliuolo VR, Dos Santos LM, Abalo A, et al. Sulfate-reducing bacteria stimulate gut immune responses and contribute to inflammation in experimental colitis. Life Sci 2017;189:29–38.
[10] Kushkevych I, Dordević D, Vítězová M. Possible synergy effect of hydrogen sulfide and acetate produced by sulfate-reducing bacteria on inflammatory bowel disease development. J Adv Res 2021;27:71–8.

[11] Singh SB, Coffman CN, Varga MG, Carroll-Portillo A, Braun CA, Lin HC. Intestinal Alkaline Phosphatase Prevents Sulfate Reducing Bacteria-Induced Increased Tight Junction Permeability by Inhibiting Snail Pathway. Front Cell Infect Microbiol 2022;12:882498.
[12] Watanabe D, Guo Y, Kamada N. Interaction between the inflammasome and commensal microorganisms in gastrointestinal health and disease. EMBO Mol Med 2021;13(12):e13452.
[13] Vance RE. The NAIP/NLRC4 inflammasomes. Curr Opin Immunol 2015;32:84–9.
[14] Zhao Y, Yang J, Shi J, et al. The NLRC4 inflammasome receptors for bacterial flagellin and type III secretion apparatus. Nature 2011;477(7366):596–600.
[15] Kay C, Wang R, Kirkby M, Man SM. Molecular mechanisms activating the NAIP-NLRC4 inflammasome: Implications in infectious disease, autoinflammation, and cancer. Immunol Rev 2020;297(1):67–82.
[16] Duncan JA, Canna SW. The NLRC4 Inflammasome. Immunol Rev 2018;281 (1):115–23.
[17] Bauer R, Rauch I. The NAIP/NLRC4 inflammasome in infection and pathology. Mol Aspects Med 2020;76:100863.
[18] Rauch I, Deets KA, Ji DX, et al. NAIP-NLRC4 Inflammasomes Coordinate Intestinal Epithelial Cell Expulsion with Eicosanoid and IL-18 Release via Activation of Caspase-1 and -8. Immunity 2017;46(4):649–59.
[19] Steiner A, Reygaerts T, Pontillo A, et al. Recessive NLRC4-Autoinflammatory Disease Reveals an Ulcerative Colitis Locus. J Clin Immunol 2022;42 (2):325–35.
[20] Bulek K, Zhao J, Liao Y, et al. Epithelial-derived gasdermin D mediates nonlytic IL-1β release during experimental colitis. J Clin Invest 2020;130(8):4218–34.
[21] Lv Q, Xing Y, Liu J, et al. Lonicerin targets EZH2 to alleviate ulcerative colitis by autophagy-mediated NLRP3 inflammasome inactivation. Acta Pharm Sin B 2021;11(9):2880–99.
[22] Man SM. Inflammasomes in the gastrointestinal tract: infection, cancer and gut microbiota homeostasis. Nat Rev Gastroenterol Hepatol 2018;15 (12):721–37.
[23] Broz P, Pelegrín P, Shao F. The gasdermins, a protein family executing cell death and inflammation. Nat Rev Immunol 2020;20(3):143–57.
[24] Chen LZ, Zhang XX, Liu MM, et al. Discovery of Novel Pterostilbene-Based Derivatives as Potent and Orally Active NLRP3 Inflammasome Inhibitors with Inflammatory Activity for Colitis. J Med Chem 2021;64(18):13633–57.
[25] Chang YW, Huang WC, Lin CY, Wang WH, Hung LC, Tellimagrandin II CYH. A Type of Plant Polyphenol Extracted from Trapa bispinosa Inhibits Antibiotic Resistance of Drug-Resistant Staphylococcus aureus. Int J Mol Sci 2019;20(22).
[26] Lin CY, Kao SH, Hung LC, et al. Lipopolysaccharide-Induced Nitric Oxide and Prostaglandin E2 Production Is Inhibited by Tellimagrandin II in Mouse and Human Macrophages. Life (Basel) 2021;11(5).
[27] Turner D, Ricciuto A, Lewis A, et al. STRIDE-II: An Update on the Selecting Therapeutic Targets in Inflammatory Bowel Disease (STRIDE) Initiative of the International Organization for the Study of IBD (IOIBD): Determining Therapeutic Goals for Treat-to-Target strategies in IBD. Gastroenterology 2021;160(5):1570–83.
[28] Haifer C, Paramsothy S, Kaakoush NO, et al. Lyophilised oral faecal microbiota transplantation for ulcerative colitis (LOTUS): a randomised, double-blind, placebo-controlled trial. Lancet Gastroenterol Hepatol 2022;7(2):141–51.
[29] Jukic A, Bakiri L, Wagner EF, Tilg H, Adolph TE. Calprotectin: from biomarker to biological function. Gut 2021;70(10):1978–88.
[30] Ricciuto A, Griffiths AM. Clinical value of fecal calprotectin. Crit Rev Clin Lab Sci 2019;56(5):307–20.
[31] Hong Y, Sheng L, Zhong J, et al. Desulfovibrio vulgaris, a potent acetic acid-producing bacterium, attenuates nonalcoholic fatty liver disease in mice. Gut Microbes 2021;13(1):1–20.
[32] Shin HS, Satsu H, Bae MJ, et al. Anti-inflammatory effect of chlorogenic acid on the IL-8 production in Caco-2 cells and the dextran sulphate sodium-induced colitis symptoms in C57BL/6 mice. Food Chem 2015;168:167–75.
[33] Zhang Y, Liu Q, Yu Y, Wang M, Wen C, He Z. Early and Short-Term Interventions in the Gut Microbiota Affects Lupus Severity, Progression, and Treatment in MRL/lpr Mice. Front Microbiol 2020;11:628.
[34] Lei Y, Tang L, Liu S, et al. Parabacteroides produces acetate to alleviate heparanase-exacerbated acute pancreatitis through reducing neutrophil infiltration. Microbiome 2021;9(1):115.
[35] Samardžić S, Arsenijević J, Božić D, Milenković M, Tešević V, Maksimović Z. Antioxidant, anti-inflammatory and gastroprotective activity of Filipendula ulmaria (L.) Maxim. and Filipendula vulgaris Moench. J Ethnopharmacol 2018;213:132–7.
[36] Tsuji T, Naito Y, Takagi T, et al. Role of metallothionein in murine experimental colitis. Int J Mol Med 2013;31(5):1037–46.
[37] Zhong XS, Winston JH, Luo X, et al. Neonatal Colonic Inflammation Epigenetically Aggravates Epithelial Inflammatory Responses to Injury in Adult Life. Cell Mol Gastroenterol Hepatol 2018;6(1):65–78.
[38] Tsai CS, Lin YW, Huang CY, et al. Thrombomodulin regulates monocye differentiation via PKCδ and ERK1/2 pathway in vitro and in atherosclerotic artery. Sci Rep 2016;6:38421.
[39] Gram AM, Wright JA, Pickering RJ, et al. Salmonella Flagellin Activates NAIP/NLRC4 and Canonical NLRP3 Inflammasomes in Human Macrophages. J Immunol 2021;206(3):631–40.
[40] Ozsolak F, Milos PM. RNA sequencing: advances, challenges and opportunities. Nat Rev Genet 2011;12(2):87–98.
[41] Graham L, Orenstein JM. Processing tissue and cells for transmission electron microscopy in diagnostic pathology and research. Nat Protoc 2007;2 (10):2439–50.
[42] Zhong W, Sun B, Gao W, et al. Salvianolic acid A targeting the transgelin-actin complex to enhance vasoconstriction. EBioMedicine 2018;37:246–58.
[43] Vijay-Kumar M, Bovilla VR, Yeoh BS, Gewirtz„ et al. Bacterial flagellin is a dominant, stable innate immune activator in the gastrointestinal contents of mice and rats. Gut Microbes 2023;15:1.
[44] Humbel F, Rieder JH, Franc Y, et al. Association of Alterations in Intestinal Microbiota With Impaired Psychological Function in Patients With Inflammatory Bowel Diseases in Remission. Clin Gastroenterol Hepatol 2020;18(9):2019–2029.e11.
[45] Tran HQ, Ley RE, Gewirtz AT, Chassaing B. Flagellin-elicited adaptive immunity suppresses flagellated microbiota and vaccinates against chronic inflammatory diseases. Nat Commun 2019;10(1):5650.
[46] Ma C, Yang D, Wang B, et al. Gasdermin D in macrophages restrains colitis by controlling cGAS-mediated inflammation. Sci Adv 2020;6(21):eaaz6717.
[47] Błażejewski AJ, Thiemann S, Schenk A, et al. Microbiota Normalization Reveals that Canonical Caspase-1 Activation Exacerbates Chemically Induced Intestinal Inflammation. Cell Rep 2017;19(11):2319–30.
[48] Winter SE, Winter MG, Xavier MN, et al. Host-derived nitrate boosts growth of E. coli in the inflamed gut. Science 2013;339(6120):708–11.
[49] Al Mamun A, Wu Y, Monalisa I, et al. Role of pyroptosis in spinal cord injury and its therapeutic implications. J Adv Res 2021;28:97–109.
[50] Burdette BE, Esparza AN, et al. Gasdermin D in pyroptosis. Acta Pharm Sin B 2021 Sep;11(9):2768–82.
[51] Katoh M, Katoh M. Identification and Characterization of Human DFNA5L, Mouse Dfna5l, and Rat Dfna5l Genes in Silico. Int J Oncol 2004;25:765–70.
[52] Rieckmann JC, Geiger R, Hornburg D, Wolf T, Kveler K, Jarrossay D, et al. Social Network Architecture of Human Immune Cells Unveiled by Quantitative Proteomics. Nat Immunol 2017;18:583–93.
[53] Wu C, Lu W, Zhang Y, Zhang G, Shi X, Hisada Y, et al. Inflammasome activation triggers blood clotting and host death through pyroptosis. Immunity 2019;50:1401–11.
[54] Shi J, Zhao Y, Wang K, Shi X, Wang Y, Huang H, et al. Cleavage of GSDMD by inflammatory caspases determines pyroptotic cell death. Nature 2015 Oct 29; 526(7575): 660–5.
[55] Liu Z, Wang M, Wang X, et al. XBP1 deficiency promotes hepatocyte pyroptosis by impairing mitophagy to activate mtDNA-cGAS-STING signaling in macrophages during acute liver injury. Redox Biol 2022;52:102305.
[56] Wang C, Yang T, Xiao J, et al. NLRP3 inflammasome activation triggers gasdermin D-independent inflammation. Sci Immunol 2021;6(64):eabj3859.
[57] Swanson KV, Deng M, Ting JP. The NLRP3 inflammasome: molecular activation and regulation to therapeutics. Nat Rev Immunol 2019;19(8):477–89.
[58] Shimamura Y, Aoki N, Sugiyama Y, Tanaka T, Murata M, Masuda S. Plant-Derived Polyphenols Interact with Staphylococcal Enterotoxin A and Inhibit Toxin Activity. PLoS One 2016;11(6):e0157082.
[59] Yasuda M, Ikeoka M, Kondo SI. Skin-related enzyme inhibitory activity by hydrolyzable polyphenols in water chestnut (Trapa natans) husk. Biosci Biotechnol Biochem 2021;85(3):666–74.